ROLE OF MIDDLE-SCALE SOLAR WIND STRUCTURES IN THE TURBULENCE DEVELOPMENT BEHIND THE BOW SHOCK

© 2025 L. S. Rakhmanova*, M. O. Riazantseva, A. A. Khokhlachev***,**
Yu. I. Yermolaev**, G. N. Zastenker*****
Space Research Institute of the Russian Academy of Sciences, Moscow, Russia
**e-mail: rakhlud@gmail.com*
***e-mail: orearm@gmail.com*
****e-mail: aleks.xaa@yandex.ru*
*****e-mail: yermol@iki.rssi.ru*
******e-mail: gzastenk@iki.rssi.ru*

Received March 08, 2024
Revised May 16, 2024
Accepted July 25, 2024

Abstract. Present study estimates contribution of the middle-scale solar wind structures (variations which are registered by a spacecraft during ~10 min intervals) in the turbulence development in the transition region behind the bow shock. The analysis is based on simultaneous measurements of plasma and/or magnetic field parameters in the solar wind, in the dayside magnetosheath and at the flanks. The study adopts measurements by Wind, THEMIS and Spektr-R spacecraft. Properties of magnetic field and ion flux fluctuation spectra are analyzed in the frequency range 0.01-4 Hz, which corresponds to transition from MHD to kinetic scales. The dynamics of turbulence properties in the magnetosheath is governed by large-scale disturbances while structures with smaller scales have effect during absence of large-scale structures.

Keywords: *solar wind, magnetosheath, plasma, turbulence, space weather*

DOI: 10.31857/S00167940250603e2

1. INTRODUCTION

The interaction between the solar wind (SW) and the Earth's magnetosphere is a complex process, in which the transition region behind the near-Earth shock wave (NESW), the magnetospheric layer (MSL), plays an important role. Models of the magnetospheric response to interplanetary perturbations use as input parameters measurements in the NE, but before the magnetopause, the plasma and magnetic field properties, including the characteristics of their variations, can be very different from the unperturbed NE. As shown by a number of studies, modification of plasma and magnetic structures coming from the NE occurs in the MSL [Rakhmanova et al., 2016]; [Turc et al., 2017]. In particular, just before the magnetopause, some of the most geoeffective parameters − sign and modulus of the *Bz* component of the magnetic field may differ from those observed in the NE [Turc et al., 2017]; [Pulinec et al., 2014]; [Šafránková et al., 2009].

It is well known that large-scale perturbations in the solar wind, such as coronal mass ejections (ICMEs) and regions of compression in front of high-velocity flows from coronal holes (CIRs), are the most geoeffective events [Yermolaev et al., 2012]. The enhanced effect on the magnetosphere is usually due to the presence in such structures of long periods of the southern orientation of the interplanetary magnetic field ($Bz < 0$), as well as to an increase in the dynamic pressure or the magnitude of the energy flux (Poynting vector) in such events [Yermolaev et al., 2012]. However, a detailed analysis shows that the internal structure of large-scale NE perturbations may also matter. For example, there may be a compression region in front of the ICME, which may be preceded by a shock wave, and such ICMEs have different geoeffectiveness [Yermolaev et al., 2012]. Various discontinuities also form within the compression region, each of which can cause a magnetospheric response [Blum et al., 2021]. Various perturbations in the NE are accompanied by peculiarities in the processes behind the ICME, in particular, the interaction of the compression region with the magnetosphere is characterized by an increased generation of jets (structures with sizes on the order of the Earth radius, characterized by a sharp increase in the plasma density) in the ICL [LaMoury et al., 2020], which have an additional impact on the magnetopause [Dmitriev et al., 2021]. The internal structure of the ICME also has its own dynamics, and the intersection of the ROMS has an impact on these dynamics. As shown in [Turc et al., 2017], the sign of the *Bz* component of the magnetic field can be reversed on time intervals of the order of 30 minutes when crossing the ICME inside magnetic clouds. Thus, the geoeffectiveness of large-scale solar wind perturbations (having spatial scales of the order of 10^7 km) can be determined by nested structures of smaller scales (variations with scales of the order of 10^5 km, registered for a time of the order of units to tens of minutes, hereinafter referred to as medium-scale structures), as well as by their modification in the ISL. Such structures in the NE are usually discontinuities of various types [Tsurutani et al., 2010]. In the framework of analyzing

solar-terrestrial relations, it is important to have an idea of how structures of different scales can be modified in the ISL and what factors influence this process.

There are several approaches to study the processes occurring in the MSL at different scales, such as analyzing individual structures [Rakhmanova et al., 2016]; [Rakhmanova et al., 2018]; [Turc et al., 2017], analyzing the averaged values of parameter variations [Nemecek et al., 2000]; [Shevyrev et al., 2003], analyzing the contribution of different wave modes [Anderson et al., 1996]; [Breuillard et al., 2016]. One approach is to analyze the spectrum of turbulent fluctuations of plasma parameters and magnetic field and the dependence of its characteristics on external factors. This approach allows us to consider a set of processes in a certain range of scales, as well as the interaction of structures of different scales among themselves. The spectra give an idea of the processes responsible for energy transfer in the turbulent cascade. The characteristics of turbulence in the NE have been most extensively studied so far [Bruno and Carbone, 2013]; [Alexandrova et al., 2013]. It is believed that on scales larger than 10^6 km, energy enters the system due to large-scale structures arising in the solar corona, energy is transferred to smaller scales through nonlinear interactions of turbulent vortices, forming the inertial region of the cascade, and on scales of the order of the proton gyroradius (~ 10^3 km), energy dissipation begins and plasma heating occurs. Experimental studies show that on the energy arrival scales the spectrum of magnetic field fluctuations is characterized by a step function f^{-1} [Bruno et al., 2009], while at the transition to the inertial region of the cascade (the so-called MHD scales) the spectrum is described by a step function $f^{5/3}$ (corresponding to the classical Kolmogorov spectrum) [Bruno et al, 2009]; [Smith et al., 2006] and at subionic (kinetic) scales there is a transition to the dissipation region, where the degree exponent lies in the range from -2 to -4 [Alexandrova et al., 2012]; [Smith et al., 2006]. The degree index is determined by the dissipation processes occurring in the plasma, e.g., Landau damping, intermittency, and the presence of plasma and magnetic structures such as thin current layers or Alvenov vortices. In addition, the characterization of spectra on kinetic scales is influenced by wave processes [Breuillard et al., 2016].

The plasma and magnetic field turbulence in the ISL has been studied to a lesser extent than in the NE due to the significantly more complicated dynamics of the processes in this region. Compared to the quiet NE, turbulence in the ISL is constantly developing in the presence of boundaries, i.e., the OZUV and the magnetopause. In addition, the processes inside the ISL, including the formation of the turbulent cascade, are significantly affected by the direction of the interplanetary magnetic field relative to the EOM: at the angle $\theta_{BN} < 45°$ between the vector of the interplanetary magnetic field and the local normal to the EOM (quasi-parallel EOM), the power of fluctuations in the ISL increases significantly [Shevyrev et al,. 2005], while at $\theta_{BN} > 45°$ (quasi perpendicular to the EOM) the power of fluctuations in the MSL is much smaller (of the order of 10% of the parameter value), but a significant temperature anisotropy is observed, leading to the generation of wave processes [Schwartz

et al., 1996]. Experimental studies show that behind the RAM, the fluctuation spectrum on MHD scales differs significantly from the Kolmogorov form [Czaykowska et al., 2001]; [Huang et al., 2017]. It is assumed that the mixing of the fluctuation phases occurs at the OZUV, and as a result, no inertial cascade region is observed in the daytime MSL, and in the process of plasma propagation to the flanks, a turbulent cascade develops and the classical Kolmogorov spectrum is formed [Huang et al., 2017]. However, a number of studies show that such a change is not always observed [Rakhmanova et al., 2019] and depends on the parameters of the impinging NE flow [Rakhmanova et al. 2020, 2022]. In particular, it is shown that during periods of quiescent NE flow, the spectra of fluctuations in the MSL are close to those observed in the NE, whereas during periods of large-scale perturbations in the interplanetary medium (ICME, CIR), a strong change in the turbulence characteristics, including the absence of Kolmogorov scaling on the MHD scales and a twisting of the spectra on kinetic scales, occurs on the OZUW.

At present, there is an idea of the properties of turbulence in different regions of the MSL [Huang et al., 2017]; [Rakhmanova et al., 2018]; [Rakhmanova et al., 2018]; [Li et al., 2020], derived from the statistical analysis of measurements behind the OZUW. In addition, there are experimental indications of the peculiarities of turbulence formation behind the OZUV for different large-scale types of NE [Rakhmanova et al., 2018]; [Rakhmanova et al., 2022]. However, as shown above, within large-scale interplanetary perturbations, there are always medium-scale structures that are subject to changes at the OZUW. By structures in this case we mean rapid changes in magnetic field (rotation) or plasma parameters or their variations. Sharp rotations of the magnetic field accompanied by changes in plasma parameters are known to be characteristic of such phenomena in the NE as tangential and rotational discontinuities [Tsurutani et al., 2010]. The influence of such structures on the turbulent cascade dynamics in the ISL has not been investigated so far, despite the contribution to solar-terrestrial coupling mentioned in the literature [Blum et al., 2021].

In the present work, based on several events, we analyze how medium-scale structures can influence the process of turbulent cascade modification at the MSL. Events are considered when measurements are available on three satellites, in the NE, in the daytime MSL, and on the flank of the MSL. Data from the Wind, THEMIS, and Spektr-R satellites are used. In order to evaluate the difference between quiet and perturbed conditions in the NE, periods of slow unperturbed NE and ICME, including the compression regions in front of them, are extracted. The characteristics of the Fourier spectra of the fluctuations of the magnetic field modulus and ion flux in the frequency range of 0.01-4 Hz are analyzed.

2. DATA

In this work, we used simultaneous measurements on three satellites located in different regions of near-Earth space, taking into account the time of plasma propagation between the satellites. In the NE, data from the Wind satellite were used: plasma characteristics were measured with the SWE instrument [Ogilvie et al., 1995] at 92 s resolution or the 3DP instrument [Lin et al., 1995] at 3 s resolution, the modulus and magnetic field components were measured with the MFI instrument [Lepping et al., 1995] at 0.092 s temporal resolution. The MSL used measurements from one of the THEMIS mission satellites, the plasma parameters were measured with the ESA instrument [Auster et al., 2008] with a resolution of 3-4 s, the magnetic field characteristics were measured with the FGM instrument [McFadden et al., 2008] with a resolution of 0.25 s.

It should be noted that in the case of the Wind and THEMIS satellites, high temporal resolution magnetic field measurements were key in the present analysis, while the plasma parameters were used as auxiliary, in particular for plasma tracing between satellites.

In addition, the MSL used data from the BMSV instrument [Zastenker et al., 2013]; [Šafránková et al., 2009] on the Spectr-R satellite. Measurements of plasma density, velocity, and temperature with a temporal resolution of 3 s and ion flux measurements with a resolution of 0.031 s were used.

Three time intervals belonging to different days were selected: 1) quiet NE, 2) the compression region before ICME, 3) ICME together with the compression region before it. The main criterion for the selection of events was the simultaneous presence of measurements with the maximum available temporal resolution on all three satellites, as well as the interval duration of at least 2 h. Events were considered when similar time series of density variations were observed on the three satellites, which guarantees consideration of the same plasma at three points. All selected events belonged to the MSL behind the quasi-perpendicular RAMS.

Fig. 1.

Fig. 1*a* shows the plasma density measurements on the Wind (NE, dark gray line), Spectrum-R (daytime MSL, light gray line), and THEMIS-C (flank, black line) satellites. The left ordinate axis refers to Wind and THEMIS-C measurements, while the right axis refers to Spectr-R measurements. The location of the satellites in near-Earth space is given in panel (*d*), the RAMS and magnetopause are shown schematically.

The main problem in analyzing multi-satellite measurements is the determination of the plasma propagation time between spacecraft. In this work, in the first step, the shear was calculated as the distance between satellites divided by the NE plasma velocity. Next, the plasma and\or magnetic field structures seen on all satellites were manually determined, and the time series of data were shifted so that the structures matched. For the example shown in Fig. 1, the time shift between Wind and Spectrum-R was 3590 s, and between Spectrum-R and THEMIS-C was 1545 s. In Fig. 1*a*, a number

of structures are clearly visible on all three satellites (e.g., density increases at~ 17:50 UT, ~ 18:10 UT).

Fig. 2.

Fig. 2 panels *b, c* show the magnetic field measurements at THEMIS-C and Wind, respectively, shifted by the same time as the plasma density time series. There are no magnetic field measurements on the Spectrum-R satellite. It is well established that the same magnetic field structures (e.g., ~ 17:50 UT,~ 18:45 UT) are observed on a pair of satellites despite the significant distance between them. A more detailed description, peculiarities, and problems of comparing data from multiple satellites in NE and MSL are given in [Rakhamnova et al., 2022].

To analyze the influence of medium-scale structures on the turbulence characteristics, we selected from the selected time series the intervals during which the indicated structures were recorded on all three satellites, as well as quasi stationary intervals during which the structures were not observed. Three selected intervals are highlighted in Fig. 1*a* − *c* were chosen to provide enough points for Fourier analysis and are ~ 17 min for the Spectrum-R and THEMIS data and 25 min for the Wind data. The difference in the interval durations is due to the different temporal resolution of the analyzed data; however, the midpoints of the Wind and THEMIS-C/Spectrum-R data intervals coincide. During intervals 1 and 3, field rotations (abrupt change of one of the components) and plasma density changes are observed. During interval 2, the plasma and magnetic field on all three satellites are quasi stationary.

It should be noted that within the framework of this work, structures with plasma density changes accompanied by magnetic field rotations are considered as medium-scale structures. The type of these structures is not analyzed.

The Fourier spectra of fluctuations of the magnetic field modulus (from Wind and THEMIS data) and ion flux (from Spectr-R data) were calculated for the intervals selected in this way. The variations of both parameters are compressional variations, and their spectra have generally the same scaling [Chen, 2016]; [Chen and Boldyrev, 2017]; [Breuillard et al., 2018]. To compare different parameters with each other, the spectra of magnetic field fluctuations and ion flux were normalized to the mean value of the parameter over the interval.

3. RESULTS

The example presented in Fig. 1 refers to the period of slow unperturbed CB (*Slow* type according to the catalog [Ermolaev et al., 2009]). Fig. *2a− c* shows the spectra for the three selected intervals, with each panel showing three spectra - in the NE (dark gray line, magnetic field modulus fluctuations $|B|$), in the daytime part of the MSL (light gray line, ion flux fluctuations $|F|$), and on the MSL flank (black line, magnetic field modulus fluctuations $|B|$). The dashed lines represent the results of approximation of the spectra by degree functions. In this paper, the Fourier spectra are

calculated using different parameters - magnetic field modulus and ion flux - due to the absence of magnetic field measurements on the Spectr-R satellite. Ion flux fluctuations represent density fluctuations, since the magnitude of the plasma velocity varies to a lesser extent (a direct comparison of the spectra of ion flux fluctuations and plasma density fluctuations was performed in [Pitňa et al. 2016]). The fluctuations of the plasma density and magnetic field modulus represent the compression component of the turbulent cascade and generally have close characteristics. Moreover, the same scaling of the magnetic field modulus and density has been shown from simultaneous measurements on the same satellite for both MHD [e.g., Chen 2016] and kinetic scales [Chen and Boldyrev 2017; Breuillard et al. 2018]. Therefore, in the present work, it is believed that a comparison of properties of the fluctuation spectra of the mentioned quantities is justified if only the fluctuation scaling, and not their power, is considered.

Interval 1 is characterized by the spectrum $\sim f^{1.7\pm0.2}$ in the NE on MHD scales and $f^{2.7\pm0.1}$ on kinetic scales. On MHD scales, the spectrum is close to the Kolmogorov form characteristic of the NE plasma. On kinetic scales, the slope of the spectrum also corresponds to the average values for the NE and is close to the value of -8/3 predicted by some theories [Boldyrev and Perez, 2012]. Behind the OZUV, a significant flattening of the spectrum on MHD scales is observed, with the slope of the spectrum being -1±0.3, which is characteristic of daytime turbulence in the magnetolayer [Czaykowska et al., 2001]; [Huang et al., 2017]. At kinetic scales, the spectrum has a slope of -2.6±0.1, close to -8/3 and to that observed in the NE. On the flanks, it is impossible to determine the slope of the spectrum on MHD scales due to the presence of a peak on transient scales caused by wave processes. At the same time, the spectrum has a slope of -2.1±0.3 on kinetic scales, i.e., the spectrum is flatter than in the NE and in the daytime MSL. Thus, in this event, the significant change in the scaling of the turbulent cascade on the MHD scales and preservation on the kinetic scales, which is expected in this region, occurred at the OZUV, while the propagation to the flanks resulted in a flattening of the kinetic part of the spectrum, which can be caused by the intensification of compression fluctuations.

The turbulence characteristics for other intervals were compared similarly. As can be seen from Fig. *2b*, for interval 2, where there are no medium-scale structures, the NE shows a slope of -1.8±0.2 on MHD scales, which is close to Kolmogorov scaling, while the slope on kinetic scales is -2.3±0.1, which is close to -7/3, also often predicted in theories [Schekochihin et al., 2009]. In the daytime MSL, the enhancement of wave activity leads to the appearance of a broad peak in the spectrum at frequencies 0.05-0.8 Hz, which makes it impossible to determine the slope on MHD scales. In the frequency region after the kink, the slope of the spectrum is -2.1±0.1, which is quite rare both in MSL and NE. Thus, a slight flattening of the spectrum on kinetic scales is observed behind the MSL. When propagating to the flanks, the peak in the spectrum is preserved, indicating the localization of the

wave process responsible for it. On kinetic scales, there is a recovery of the slope of the spectrum -2.3±0.2, close to that observed in the NE.

For interval 3, during which medium-scale structures are recorded, a slope of -1.6±0.1 on MHD scales, i.e., the Kolmogorov spectrum, and -2.3±0.1 on kinetic scales is observed in the NE. In the daytime MSL, the spectrum flattens to $f^{1.2\pm0.3}$ on MHD scales, while on kinetic scales the spectrum does not change and has a slope of -2.3±0.1. On the flanks of the MSL- on MHD scales, the spectrum is characterized by a slope of -0.8±0.1, i.e., also different from the Kolmogorov spectrum. On kinetic scales, the slope of the spectrum is -2.4±0.1, which is close to the observations in the NE and in the daytime MSL.

Thus, under quiet conditions in the NE in the absence of medium-scale structures (interval 2) in the daytime MSL, the main contribution to the spectra of turbulent fluctuations on MHD scales is made by wave processes, which leads to the dominance of the peak in the spectrum at frequencies close to the kink. On kinetic scales, the spectra flatten slightly behind the RAM to degree indices, which are observed statistically quite rarely. When propagating towards the flanks, the peak in the spectrum is preserved, implying that the source of the wave process moves towards the flanks together with the plasma. On kinetic scales, the recovery of the spaling characteristic of the CB is observed. It should be noted that, as a rule, either ion-cyclotron Alvenov instabilities or mirror mode waves, which are compression variations, are observed in MSLs. It can be assumed that the general low level of fluctuations leads to the fact that after the crossing of the MSL, the main contribution to the development of the turbulent cascade is given by the compression mirror mode.

In the presence of medium-scale structures (intervals 1, 3), the Kolmogorov scaling, which is characteristic of turbulence in the NE, disappears on the MHD scales behind the OZUV, which is on average typical of the daytime MSL [Huang et al., 2017]. At kinetic scales, however, the slope of the spectrum is preserved in the daytime MSL. However, when propagating towards the flanks, there is no recovery of the Kolmogorov scaling, which typically occurs when the plasma moves away from the sunlit region of the MSL [Rakhmanova et al., 2022]. In addition, a flattening of the spectra can be observed on kinetic scales. It is worth noting that in this case, a peak of compressional fluctuations was also present at the spectrum break frequencies.

Fig. 3.

In Fig. 3 (analogous to Fig. 1) shows the event related to the *Sheath* compression region before ICME. In the ICME region itself, the necessary measurements were not available. The THEMIS-E satellite (before 00:10 UT) and the THEMIS-A satellite (after 00:10 UT) were located in the daytime part of the ICLE. Four intervals can be distinguished during the event: in intervals 1 and 3, both in the NE and in the MSL, significant density variations and magnetic field rotations (accompanied by a change in the sign of the *Bz* component) are observed; in intervals 2 and 4, despite the presence of

variations of all magnetic field components, typical for NE of this type, no change in the sign of *Bz* is observed, and there are no significant variations in the plasma density. In this event, intervals 1 and 3 were considered as intervals with medium-scale structures, events 2 and 4− as quasi stationary intervals without structures.

Fig. 4.

Similarly, Fig. 4 shows the event of February 16, 2014, in which it is possible to perform an analysis for both the *Sheath* region and the ICME (magnetic cloud, MC) before which this region formed. Intervals 1 and 3 are characterized by the absence of structures, while intervals 2 and 4 contain medium-scale structures. As can be seen from Fig. 4, the temporal shift that ensures the coincidence of structures in the *Sheath* region leads to a divergence of magnetic structures in the MC region (at 05:00-05:30 UT). This is due to the difference in the propagation velocity of the different CB structures. In this case, for each of the considered intervals, the shift between the data time series was refined separately.

The approximation of the obtained spectra was carried out similarly to the case of quiet CB. Characteristics of spectra for all considered intervals are given in Table 1.

Table 1.

Table 1 shows the sequence number of the interval, the date of the event, the type of SV and the number of the interval in the figure, the presence of medium-scale structures within the interval, and the values of the slopes of the spectra in the three regions of near-Earth space on both MHD and kinetic scales. In some cases, determination of the slope on MHD scales is impossible due to wave processes.

As shown by comparing the slopes of the spectra at different locations for the perturbed NE, there is usually strong wave activity in the daytime MSL at the MHD scales that interferes with the determination of the scaling. However, the intervals 4− 7 are characterized both by the preservation of scaling on MHD scales at the crossing of the ROMS and by a significant flattening of the spectra, and the flattening can be observed both against the background of medium-scale structures and without them. At that, the spectra behind the LSL are characterized by a more significant flattening than for the quiet NE. Similar changes at the OZUV were observed earlier for the perturbed NE [Rakhmanova et al., 2022], and are a characteristic change in the properties of turbulence at the OZUV.

For most of the flanking events, Kolmogorov spectra at MHD scales are observed, which is characteristic of this region. For events 8 and 11, however, the spectra remain flatter than in the NE. These events are observed both in the background of the quasi stationary CB and in the presence of medium-scale structures, i.e., the indicated structures do not influence this process.

On kinetic scales, for most events (except for 6, 7), we observe a steepening of the spectra behind the OZUV, regardless of the presence of medium-scale structures. At the same time, the steepest spectra in the daytime ICME (with slopes up to -4.8) are observed during the periods of the ICME itself, which agrees well with past results [Rakhmanova et al., 2022]. For events 6 and 7, observed during periods of interaction with the MSL of *Sheath* compression regions, atypically steep spectra in the NE and their flattening in the daytime MSL are observed. Interestingly, intervals 6 and 7 are characterized by the presence and absence of medium-scale structures, respectively. That is, the processes responsible for the spectrum changes at the MSL and in this case are not related to the medium-scale structures.

On the flanks of the MSL on kinetic scales, spectra with slopes -(2.6-3.2), characteristic of MSL turbulence, are usually formed. No relationship is observed between the values of the slopes in the NE and on the flank and the presence of medium-scale structures. However, peculiarities in the spectra are observed in events 6 and 7 discussed above: they are characterized by a flattening of the spectra on the flanks to values -(2.0-2.2). This property of the compression regions (*Shearh* and CIR) was noted earlier [Rakhmanova et al., 2022], and, as can be seen from the data in Table 1, is not related to the presence of medium-scale structures.

It should be noted that for the events under consideration, the spectra of ion flux fluctuations were analyzed during periods of quiet NE on the flank, while fluctuations of the magnetic field modulus were considered during periods of perturbed NE on the flank. However, the slopes of the spectra obtained for the ion flux agree well with those obtained earlier for the magnetic field modulus fluctuations in the same region [Rakhmanova et al. 2022] also for quiet conditions in the NE. In addition, the comparison of the spectra of ion flux fluctuations and magnetic field modulus at the flank (at different distances toward the tail of the magnetosphere) from the Spektr-R and THEMIS satellites have the same scaling. Despite the difference of the measured parameters, the compressible fluctuations show the same scaling, so we can conclude that the differences revealed in this work for the quiet and perturbed NE are due to the peculiarities of the development of the compressible component of the turbulent cascade under different conditions in the NE, rather than to the difference of the parameters under consideration.

Thus, during periods of perturbed solar wind, the main changes in the turbulent cascade (such as flattening on MHD scales and significant twisting on kinetic scales) are determined by the large-scale NE type and are independent of the dynamics of structures within the large-scale perturbation.

4. CONCLUSION

In this paper, based on the comparison of simultaneous measurements at three points of near-Earth space - in the NE, in the daytime MSL and on the MSL flank - we analyzed, how the presence

of medium-scale structures (variations recorded by the satellite over times of ~10 min) can influence the dynamics of the turbulent cascade behind the OHMV. It is shown that:

1. During periods of unperturbed slow NE in the absence of medium-scale structures, the dynamics of the turbulent cascade in the MSL is determined by the wave processes arising behind the GHE.

2. During the periods of undisturbed slow SI in the presence of medium-scale structures behind the ROM, the slopes of the spectra on MHD scales close to -1 are observed, which can be related to the violation of the conditions of developed turbulence and the absence of the inertial region in the turbulent cascade; the recovery of the spectra characteristic of developed turbulence does not occur on the MSL flanks.

3. During periods of quiet slow NE, the characteristics of turbulence on kinetic scales do not change at the plasma entry into the MSL and propagation to the flanks, which indicates the universality of the energy dissipation processes before and after the MSL; in some cases, a flattening of the spectra at the plasma propagation to the flanks can be observed, probably caused by local instabilities.

4. The presence of medium-scale structures against the background of large-scale perturbations in the NE does not affect the modification of the turbulence characteristics at the LSFM: all changes− absence of Kolmogorov scaling on MHD scales and twisting of the spectra on kinetic scales in the daytime MSL and restoration of the shape close to that observed in the NE at the flanks correspond to the previously presented statistics both in the presence and absence of medium-scale structures.

Thus, it is shown that the main contribution to the development of the turbulent cascade in the LSL is made by large-scale perturbations in the solar wind. The dynamics of smaller scale structures (of the order of 10 min) may have an influence on the turbulence behind the RAMS against the background of calm conditions in the solar wind.

FUNDING

The research was supported by the Russian Science Foundation, grant No. 22-12-00227, (https://rscf.ru/project/22-12-00227/).

REFERENCES

1. *Ermolaev Yu.I., Nikolaeva N.S., Lodkina I.G., Ermolaev M.Yu.* Catalog of large-scale solar wind phenomena for the period 1976−2000 // Cosmic research. V. 47. No. 2. P. 99–113. 2009.

2. *Zastenker G.N., Shafrankova Ya., Nemechek Z., et al.* Rapid measurements of solar wind parameters using the BMSV instrument // Cosmic research. V. 51. No. 2. P. 88–99. 2013.

3. *Pulinets M.S., Ryazantseva M.O., Antonova E.E., Kirpichev I.P.* Dependence of the magnetic field parameters near the subsolar point of the magnetosphere on the interplanetary magnetic field according to the THEMIS experiment // Geomagnetism and Aeronomy. V. 52. No. 6. P. 769–778. 2012.
4. *Rakhmanova L.S., Ryazantseva M.O., Zastenker G.N., Verigin M.I., Ermolaev Yu.I., Lodkina I.G.* Influence of the parameters of the interplanetary medium and the magnetosheath boundaries on the value of the correlation coefficient between the ion flux in the solar wind and the magnetosheath // Geomagnetism and Aeronomy. V. 58. No. 4. P. 463–470. 2018.
5. *Rakhmanova L.S., Ryazantseva M.O., Zastenker G.N., Ermolaev Yu.I., Lodkina I.G., Chesalin L.S.* Influence of the characteristics of solar wind plasma turbulence on the properties of the turbulent cascade in the magnetosheath // Space Research. V. 57. No. 6. P. 1–8. 2019.
6. *Alexandrova O., Lacombe C., Mangeney A., Grappin R., Maksimovic, M.* Solar wind turbulent spectrum at plasma kinetic scales // Astrophys. J. V. 760. N 2. P. 121–126. 2012. https://doi.org/10.1088/0004-637X/760/2/121
7. *Alexandrova O., Chen C. H. K., Sorriso-Valvo L., Horbury T. S., Bale S. D.* Solar Wind Turbulence and the Role of Ion Instabilities // Space Sci. Rev. V. 178. P. 101–139. 2013. https://doi.org/10.1007/s11214-013-0004-8
8. *Anderson B.J., Fuselier S.A., Gary S.P., Denton R.E.* Magnetic spectral signatures in the Earth's magnetosheath and plasmadepletion layer // J. Geophys. Res. V. 99. P. 5877–5891. 1994. https://doi.org/10.1029/93JA02827
9. *Angelopoulos V.* The THEMIS mission // Space Sci. Rev. V. 141. P. 5–34. 2008. https://doi.org/10.1007/s11214-008-9336-1
10. *Auster H. U., Glassmeier K. H., Magnes W., et al.* The THEMIS Fluxgate Magnetometer // Space Sci. Rev. V. 141. N 1–4. P. 235–264. 2008. https://doi.org/10.1007/s11214-008-9365-9
11. *Blum L. W., Koval A., Richardson I. G., Wilson L. B., Malaspina D., Greeley A., Jaynes A. N.* Prompt response of the dayside magnetosphere to discrete structures within the sheath region of a coronal mass ejection // Geophysical Research Letters. V. 48. e2021GL092700. 2021. https://doi.org/10.1029/2021GL092700
12. *Boldyrev S., Perez J. C.* Spectrum of Kinetic Alfven Turbulence // Astrophys. J. Lett. V. 758. N 2. L44. 2012. https://doi.org/10.1088/2041-8205/758/2/L44
13. *Borodkova N., Zastenker G., Riazantseva M., Richardson J.* Large and sharp solar wind dynamic pressure variations as a source of geomagnetic field disturbances at the geosynchronous orbit // Planet. Space Sci. V. 53. P. 25−32. 2005. https://doi.org/10.1016/j.pss.2004.09.025

14. *Breuillard H., Matteini L., Argall M. R., et al.* New Insights into the Nature of Turbulence in the Earth's Magnetosheath Using Magnetospheric Multi Scale Mission Data // Astrophys. J. V. 859. 127. 2018. https://doi.org/10.3847/1538-4357/aabae8
15. *Breuillard H., Yordanova E., Vaivads A., Alexandrova O.* The effects of kinetic instabilities on small-scale turbulence in Earth's magnetosheath // Astrophys. J. V. 829. 54. 2016. https://doi.org/10.3847/0004-637X/829/1/54
16. *Bruno R., Carbone V., Vörös Z., et al.* Coordinated Study on Solar Wind Turbulence During the Venus-Express, ACE and Ulysses Alignment of August 2007 // Earth Moon Planets. V. 104. P. 101–104. 2013. https://doi.org/10.1007/s11038-008-9272-9
17. *Bruno R., Carbone V.* The Solar Wind as a Turbulence Laboratory // Living Rev. Sol. Phys. V. 10. № 2. 2013. https://doi.org/10.12942/lrsp-2013-2
18. *Chen C. H. K.* Recent progress in astrophysical plasma turbulence from solar wind observations. // J. Plasma Phys. V. 82. 535820602. 2016. https://doi.org/10.1017/S0022377816001124
19. *Chen C. H. K., Boldyrev S.* Nature of Kinetic Scale Turbulence in the Earth's Magnetosheath // Astrophys. J. V. 842. P. 122–131. 2017. https://doi.org/10.3847/1538-4357/aa74e0
20. *Czaykowska A., Bauer T. M., Treumann R. A., and Baumjohann W*. Magnetic field fluctuations across the Earth's bow shock // Ann. Geophys. V. 19. P. 275–287. 2001. https://doi.org/10.5194/angeo-19-275-2001
21. *Dmitriev A.V., Lalchand B., Ghosh S.* Mechanisms and Evolution of Geoeffective Large-Scale Plasma Jets in the Magnetosheath // Universe. V. 7. 152. https://doi.org/10.3390/universe7050152
22. *Huang S. Y., Hadid L. Z., Sahraoui F., Yuan Z. G., Deng X. H.* On the Existence of the Kolmogorov Inertial Range in the Terrestrial Magnetosheath Turbulence // Astrophys. J. Lett. V. 836. L10. 2017. https://doi.org/10.3847/2041-8213/836/1/L10
23. *Lacombe C., Belmont G.* Waves in the Earth's magnetosheath: Observations and interpretations // Adv. Sp. Res. V. 15. P. 329–340. 1995. https://doi.org/10.1016/0273-1177(94)00113-F
24. *LaMoury A. T., Hietala H., Plaschke F., Vuorinen L., Eastwood J. P.* Solar wind control of magnetosheath jet formation and propagation to the magnetopause. J. Geophys. Res. Space Phys. // V. 126. N 9. e2021JA029592. 2021. https://doi.org/10.1029/2021ja029592
25. *Lepping R. P., Acuna M. H., Burlaga L. F., et al.* The WIND magnetic field investigation // Space Sci. Rev. V. 71. N 1–4. P. 207–229. 1995. https://doi.org/10.1007/BF00751330
26. *Li H., Jiang W., Wang C., Verscharen D., Zeng C., Russell C. T., Giles B., Burch J. L.* Evolution of the Earth's Magnetosheath Turbulence: A Statistical Study Based on MMS Observations // Astrophys. J. V. 898. L43. 2020. https://doi.org/10.3847/2041-8213/aba531

27. *Lin R. P., Anderson K. A., Ashford S., et al.* Three-Dimensional Plasma and Energetic Particle Investigation for the Wind Spacecraft // Space Sci. Rev. V. 71. P. 125–153. 1995. https://doi.org/10.1007/BF00751328
28. *McFadden J.P., Carlson C.W., Larson D., Ludlam M., Abiad R., Elliott B., Turin, P., Marckwordt M., Angelopoulos V.* The THEMIS ESA plasma instrument and in-flight calibration // Space Sci. Rev. V. 141. P. 277–302. 2008. https://doi.org/10.1007/s11214-008-9440-2
29. *Němeček Z., Šafránková J., Zastenker G. N., Pišoft P., Paularena K. I., and Richardson J. D.* Observations of the radial magnetosheath profile and a comparison with gasdynamic model 1024 predictions // Geophys. Res. Lett. V. 27. P. 2801–2804. 2000. https://doi.org/10.1029/2000GL000063
30. *Ogilvie K. W., Chornay D. J., Fritzenreiter R. J., et al.* SWE, a comprehensive plasma instrument for the Wind spacecraft // Space Sci. Rev.V. 71. N 1–4. P. 55–77. 1995. https://doi.org/10.1007/BF00751326
31. *Pitňa A., Šafránková J., Němeček Z., Goncharov O., Němec F., Přech L., Chen C. H. K., Zastenker G.* Density fluctuations upstream and downstream of interplanetary shocks // Astrophys. J. V. 819. 41–50. 2016. https://doi.org/10.3847/0004-637X/819/1/41
32. *Rakhmanova L., Riazantseva M., Zastenker G., Yermolaev Y., and Lodkina I.* Dynamics of Plasma Turbulence at Earth's Bow Shock and through the Magnetosheath // Astrophys. J. V. 901. N 30. P. 30–40. 2020. https://doi.org/10.3847/1538-4357/abae00
33. *Rakhmanova L., Riazantseva M., Zastenker G. and Yermolaev Y.* Large-Scale Solar Wind Phenomena Affecting the Turbulent Cascade Evolution behind the Quasi-Perpendicular Bow Shock // Universe. V. 8. N 12. P. 611. 2022. https://doi.org/10.3390/universe8120611
34. *Rakhmanova L., Riazantseva M., Zastenker G., Verigin M.* Kinetic-Scale Ion Flux Fluctuations Behind the Quasi-Parallel and Quasi-Perpendicular Bow Shock. // J. Geophys. Res. Sp. Phys. V. 123. P. 5300–5314. 2018. https://doi.org/10.1029/2018JA025179
35. *Šafránková J., Hayosh M., Gutinska O., Němeček Z., Přech L.* Reliability of prediction of the magnetosheath Bz component from the interplanetary magnetic field observations // J. Geophys. Res. V. 114. A12213. 2009. https://doi.org/10.1029/2009JA014552
36. *Šafránková, J., Němeček, Z., Přech, L., et al.* Fast solar wind monitor (BMSW): description and first results // Space Sci. Rev. V. 175. P. 165–182. 2013. https://doi.org/10.1007/s11214-013-9979-4
37. *Schekochihin A. A., Cowley S. C., Dorland W., Hammett G. W., Howes G. G., Quataert E., Tatsuno T.* Astrophysical gyrokinetics: kinetic and fluid turbulent cascades in magnetized weakly collisional plasmas // Astrophys. J. Suppl. Ser. V. 182. P. 310–377. 2009. https://doi.org/10.1088/0067-0049/182/1/310

38. *Schwartz S. J., Burgess D., Moses J. J.* Low-frequency waves in the Earth's magnetosheath: present status // Ann. Geophys. V. 14. P. 1134–1150. 1996. https://doi.org/10.1007/s00585-996-1134-z

39. *Shevyrev N. N., Zastenker G. N., Nozdrachev M. N., Němeček Z., Šafránková J., and Richardson J. D.* High and low frequency large amplitude variations of plasma and magnetic field in the magnetosheath: radial profile and some features // Adv. Space Res. V. 31. P. 1389–1394. 2003. https://doi.org/10.1016/S0273-1177(03)00008-5

40. *Shevyrev N.N., Zastenker G. N.* Some features of the plasma flow in the magnetosheath behind quasi-parallel and quasi-perpendicular bow shocks // Planet. Space Sci. V. 53. P. 95–102. 2005. https://doi.org/10.1016/j.pss.2004.09.033

41. *Smith C., Hamilton K., Vasquez B, Leamon R.* Dependence of the dissipation range spectrum of interplanetary magnetic fluctuations on the rate of energy cascade // Astrophys. J. V. 645: L85–L88. 2006. https://doi.org/10.1086/506151

42. *Tsurutani B. T., Lakhina G. S., Verkhoglyadova O. P., Gonzalez W. D., Echer E., Guarnieri F. L.* A review of interplanetary discontinuities and their geomagnetic effects // Journal of Atmospheric and Solar-Terrestrial Physics. V. 73. N 1. P. 5–19. 2011. https://doi.org/10.1016/j.jastp.2010.04.001

43. *Turc L., Fontaine D., Escoubet C. P., Kilpua E. K. J., Dimmock A. P.* Statistical study of the alteration of the magnetic structureof magnetic clouds in the Earth's magnetosheath // J J. Geophys. Res. Sp. Phys. V. 122. N 3. P. 2956–2972. 2017. https://doi.org/10.1002/2016JA023654

44. *Verigin M. I., Tátrallyay M., Erdős G., Kotova G.A*. Magnetosheath – Interplanetary medium reference frame: Application for a statistical study of mirror type waves in the terrestrial plasma environment // Adv. Space Res. V. 37. P. 515-521. 2006. https://doi.org/10.1016/j.asr.2005.03.042

45. *Yermolaev Y. I., Nikolaeva N. S., Lodkina I. G., Yermolaev M. Y.* Geoeffectiveness and efficiency of CIR, sheath, and ICME in generation of magnetic storms // J. Geophys. Res. V. 117. A00L07. 2012. https://doi.org/10.1029/2011JA017139

Table 1. Spectra slopes in three regions of near-Earth space for the considered events.

№	Date, time	Type, № interval	Structures	MHD slope			Slope of kinet.		
				NE	Dn. MSL	Flank	CB	MSL Dn.	Flank
1	09.07.14, 17:48 UT.	*Slow*, 1	+	-1.7±0.2	-1.0±0.3	-	-2.7±0.1	-2.6±0.1	-2.1±0.3
2	09.07.14, 18:13 UT	*Slow*, 2	-	-1.8±0.2	-	-	-2.3±0.1	-2.0±0.1	-1.7±0.2
3	09.07.14, 18:40 UT	*Slow*, 3	+	-1.6±0.1	-1.2±0.3	-0.8±0.1	-2.3±0.1	-2.3±0.1	-2.4±0.2
4	07.02.14, 17:18 UT	*Sheath*, 1	+	-1.8±0.1	-2±0.3	-1.6±0.1	-2.5±0.1	-3.5±0.1	-3.0±0.1
5	07.02.14, 18:45 UT	*Sheath*, 2	-	-1.6±0.2	-0.6±0.2	-1.5±0.1	-3.2±0.1	-3.5±0.2	-2.8±0.1
6	07.02.14, 22:14 UT	*Sheath*, 3	+	-1.9±0.1	-0.5±0.2	-1.6±0.1	-4.2±0.2	-3.0±0.2	-2.0±0.1
7	08.02.14, 00:40	*Sheath*, 4	-	-1.9±0.1	-	-1.7±0.1	-3.5±0.2	-3.2±0.2	-2.2±0.1
8	16.02.14, 04:08 UT	*Sheath*, 1	-	-1.8±0.1	-	-1.4±0.1	-2.6±0.2	-3.0±0.2	-3.2±0.2
9	16.02.14, 04:22 UT	*Sheath*, 2	+	-1.6±0.1	-	-1.7±0.1	-2.9±0.2	-3.4±0.2	-2.6±0.2
10	16.02.14, 05:06 UT	MC, 3	-	-1.9±0.2	-	-1.7±0.1	-2.3±0.1	-4.1±0.2	-2.8±0.1
11	16.02.14, 05:35 UT	MC, 4	+	-1.8±0.2	-	-1.3±0.1	-2.2±0.1	-4.8±0.3	-2.6±0.1

Figure captions

Fig. 1. (*a*) - Ion flux in the NE (dark gray line), in the daytime MSL (light gray line), and on the flank (black line) for the July 09, 2014 event; (*b, c)* - measurements of the modulus and magnetic field components on THEMIS and Wind satellites, respectively, data from all satellites are shifted by the plasma propagation time; (*d*) - satellite locations for the event in question.

Fig. 2. Comparison of the normalized fluctuation spectra of the magnetic field modulus (|B|) and ion flux (|F|) in three regions of near-Earth space - in the NE (dark gray line), in the daytime MSL (light gray line), and on the flanks (black line) - for the three intervals marked in Fig. 1.

Fig. 3. Similar to Fig. 1 for the event of February 7-8, 2014, referring to the *Sheath* compression region.

Fig. 4. Similar to Fig. 1 for the February 16, 2014 event relating to ICME with the *Sheath* compression region in front of it.

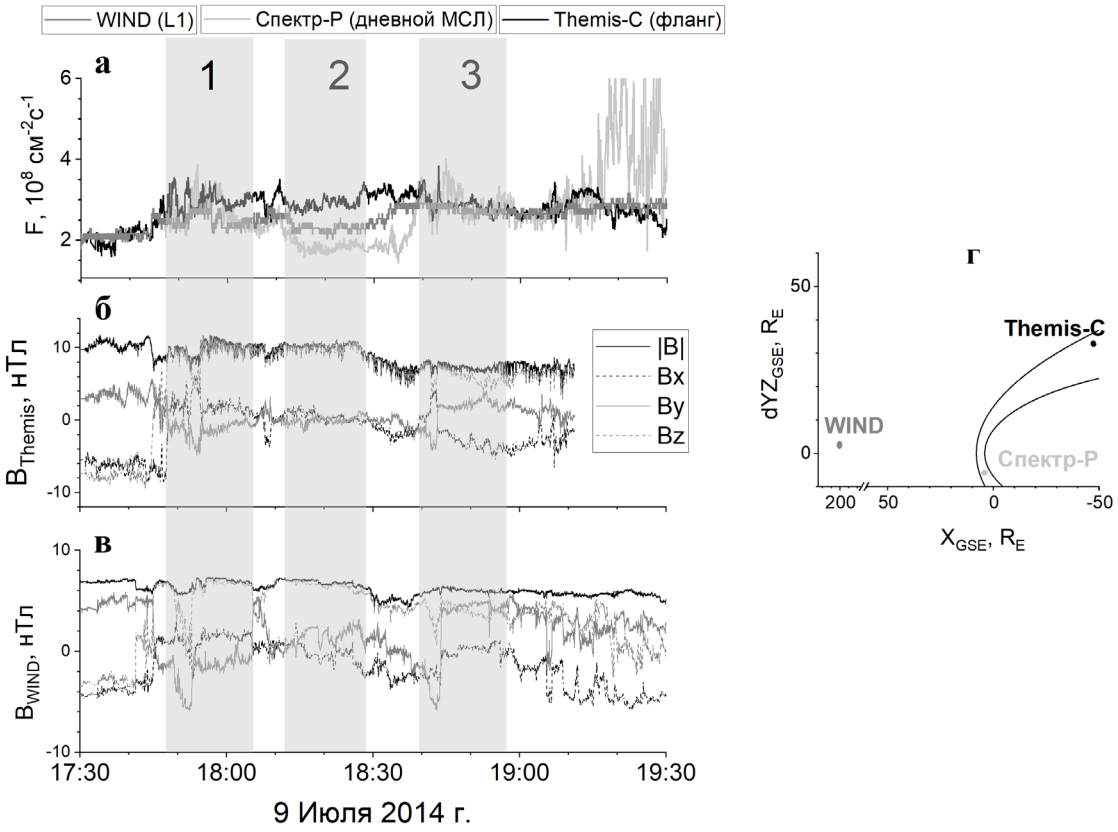
WIND (L1)
Спектр-Р (дневной МСЛ)
Themis-C (фланг)
а
1
2
3
F, 10^8 см^-2с^-1
б
B_Themis, нТл
|B|
Bx
By
Bz
в
B_WIND, нТл
17:30
18:00
18:30
19:00
19:30
9 Июля 2014 г.
г
dYZ_GSE, R_E
Themis-C
WIND
Спектр-Р
X_GSE, R_E

Fig. 1.

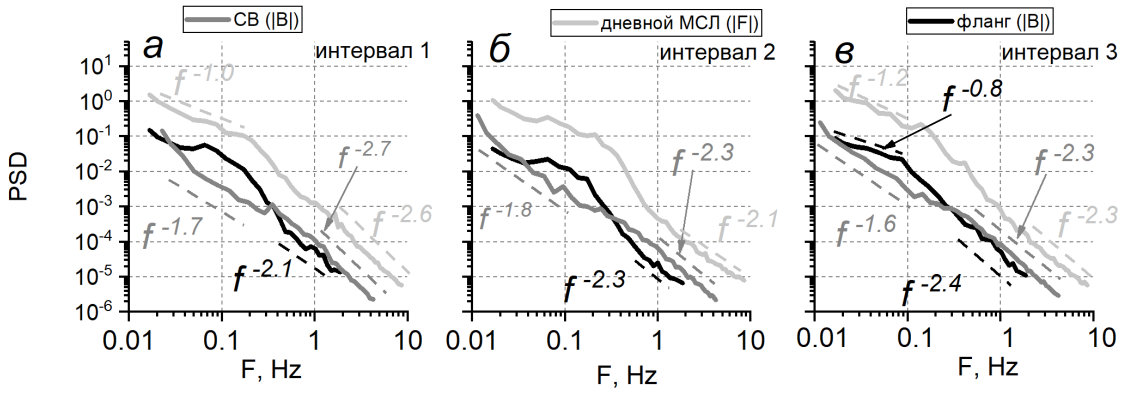
СВ (|B|)
а
интервал 1
f -1.0
f -2.7
f -2.6
f -1.7
f -2.1
дневной МСЛ (|F|)
б
интервал 2
f -2.3
f -2.1
f -1.8
f -2.3
фланг (|B|)
в
интервал 3
f -1.2
f -0.8
f -2.3
f -2.3
f -1.6
f -2.4
PSD
F, Hz
F, Hz
F, Hz

Fig. 2.

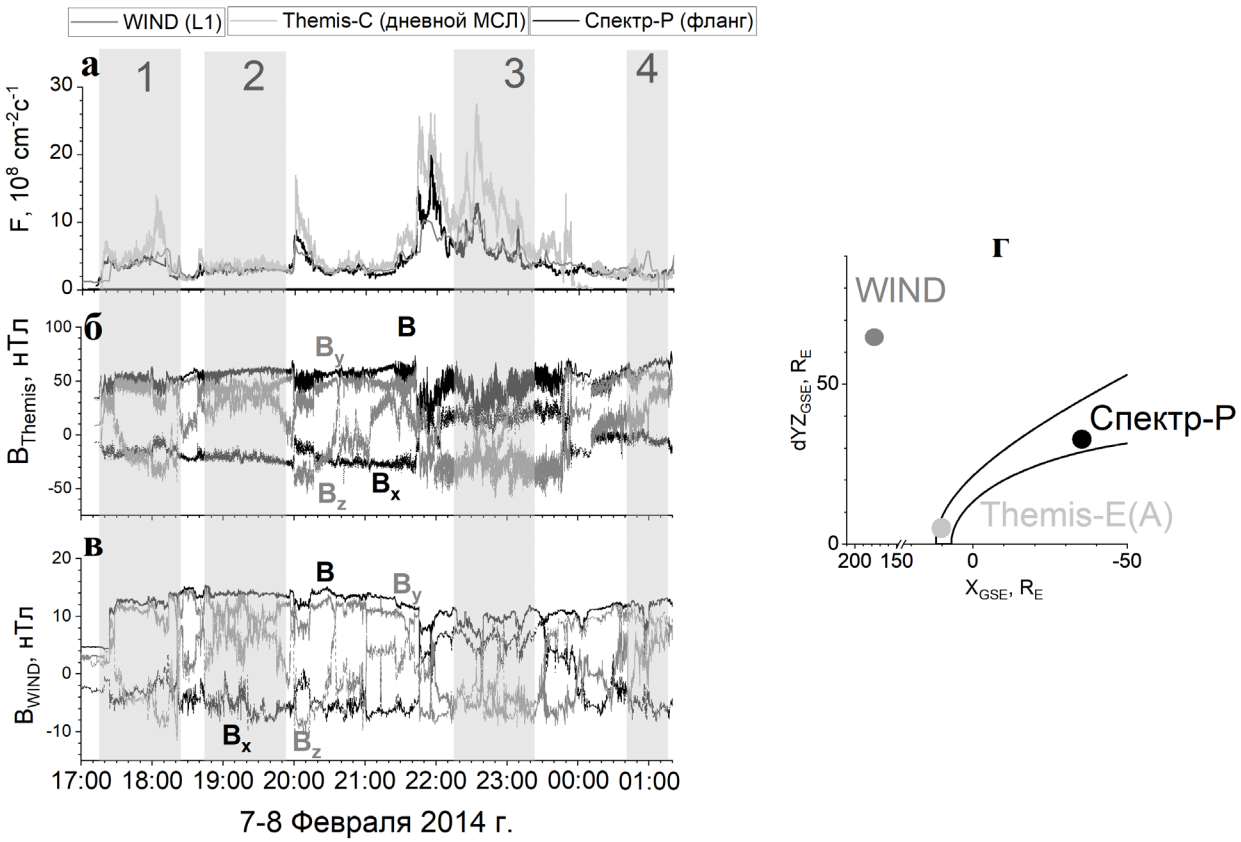
WIND (L1)
Themis-C (дневной МСЛ)
Спектр-Р (фланг)
а
1
2
3
4
F, 10^8 cm^-2c^-1
б
B
B_y
B_z
B_x
B_Themis, нТл
в
B
B_y
B_x
B_z
B_WIND, нТл
17:00 18:00 19:00 20:00 21:00 22:00 23:00 00:00 01:00
7-8 Февраля 2014 г.
г
WIND
Спектр-Р
Themis-E(A)
dYZ_GSE, R_E
X_GSE, R_E

Fig. 3.

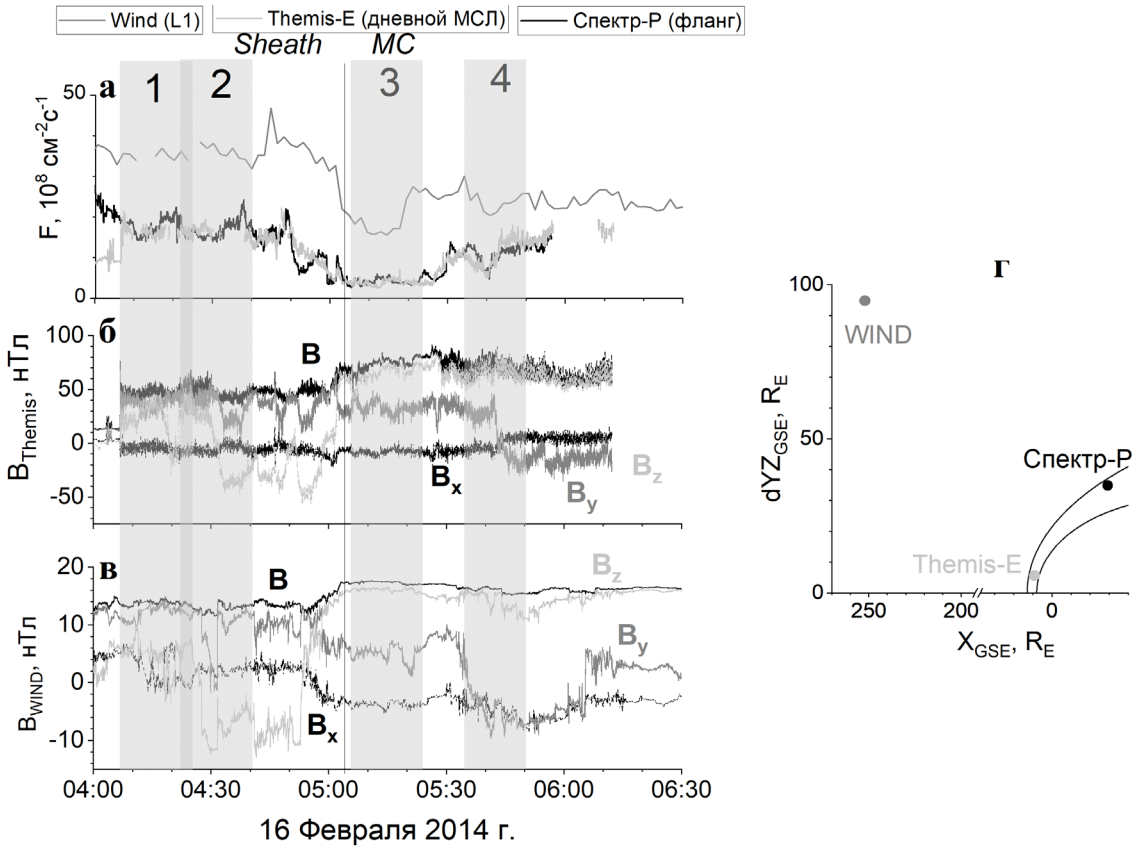
Wind (L1)
Themis-E (дневной МСЛ)
Спектр-P (фланг)
Sheath
MC
1
2
3
4
а
F, 10^8 см^-2с^-1
б
B
B_x
B_y
B_z
B_Themis, нТл
в
B_WIND, нТл
04:00
04:30
05:00
05:30
06:00
06:30
16 Февраля 2014 г.
г
WIND
Спектр-P
Themis-E
dYZ_GSE, R_E
X_GSE, R_E

Fig. 4.